Optic-null medium: realization and applications

Qiong He, Shiyi Xiao, Xin Li, and Lei Zhou*

State Key Laboratory of Surface Physics and Key Laboratory of Micro and Nano Photonic Structures (Ministry of Education), Fudan University, Shanghai 200433, China

phzhou@fudan.edu.cn

Abstract: Optic-null medium (ONM), an electromagnetic (EM) space representing optically nothing, has many interesting applications but is difficult to realize practically due to its extreme EM parameters. Here we demonstrate that a holey metallic plate with periodic array of subwavelength apertures can well mimic an ONM. We develop an effective-medium theory to extract the EM parameters of the designed ONM, and employ full-wave simulations to demonstrate its optical functionalities. Microwave experiments, in excellent agreement with full-wave simulations, are performed to illustrate several applications of the ONM, including the radiation cancellation effect and the hyperlensing effect.

OCIS codes: (230.0230) Optical devices; (260.2110) Electromagnetic optics; (160.3918) Metamaterials; (260.2065) Effective medium theory; (080.2710) Inhomogeneous optical media.

References and links

1. J. B. Pendry, D. Schurig, and D. R. Smith, "Controlling electromagnetic fields," Science **312**(5781), 1780–1782 (2006).
2. U. Leonhardt, "Optical conformal mapping," Science **312**(5781), 1777–1780 (2006).
3. Y. Lai, J. Ng, H. Y. Chen, D. Z. Han, J. J. Xiao, Z. Q. Zhang, and C. T. Chan, "Illusion optics: the optical transformation of an object into another object," Phys. Rev. Lett. **102**(25), 253902 (2009).
4. Y. Lai, J. Ng, H. Y. Chen, Z. Q. Zhang, and C. T. Chan, "Illusion optics," Front. Phys. China **5**(3), 308–318 (2010).
5. H. Y. Chen and C. T. Chan, "Transformation media that rotate electromagnetic fields," Appl. Phys. Lett. **90**(24), 241105 (2007).
6. M. Rahm, S. A. Cummer, D. Schurig, J. B. Pendry, and D. R. Smith, "Optical design of reflectionless complex media by finite embedded coordinate transformations," Phys. Rev. Lett. **100**(6), 063903 (2008).
7. W. X. Jiang, T. J. Cui, H. F. Ma, X. Y. Zhou, and Q. Cheng, "Cylindrical-to-plane-wave conversion via embedded optical transformation," Appl. Phys. Lett. **92**(26), 261903 (2008).
8. Y. Shen, K. Ding, W. Sun, and L. Zhou, "A chirality switching device designed with transformation optics," Opt. Express **18**(20), 21419–21426 (2010).
9. S. Han, Y. Xiong, D. Genov, Z. Liu, G. Bartal, and X. Zhang, "Ray optics at a deep-subwavelength scale: a transformation optics approach," Nano Lett. **8**(12), 4243–4247 (2008).
10. A. V. Kildishev and E. E. Narimanov, "Impedance-matched hyperlens," Opt. Lett. **32**(23), 3432–3434 (2007).
11. R. A. Shelby, D. R. Smith, and S. Schultz, "Experimental verification of a negative index of refraction," Science **292**(5514), 77–79 (2001).
12. D. R. Smith, J. B. Pendry, and M. C. K. Wiltshire, "Metamaterials and negative refractive index," Science **305**(5685), 788–792 (2004).
13. J. B. Pendry, "Negative refraction makes a perfect lens," Phys. Rev. Lett. **85**(18), 3966–3969 (2000).
14. N. Fang, H. Lee, C. Sun, and X. Zhang, "Sub-Diffraction-Limited optical imaging with a silver superlens," Science **308**(5721), 534–537 (2005).
15. N. Yu, P. Genevet, M. A. Kats, F. Aieta, J.-P. Tetienne, F. Capasso, and Z. Gaburro, "Light propagation with phase discontinuities: generalized laws of reflection and refraction," Science **334**(6054), 333–337 (2011).
16. S. Sun, Q. He, S. Xiao, Q. Xu, X. Li, and L. Zhou, "Gradient-index meta-surfaces as a bridge linking propagating waves and surface waves," Nat. Mater. **11**(5), 426–431 (2012).
17. COMSOL Multi-physics 3.5, developed by COMSOL ©, network license (2008).
18. In our simulations, we took $\Delta / b = 10000$.
19. Here, we only present the field distributions for TE-polarized excitation since the TM case is quite similar to the TE case.
20. A. Alù, M. G. Silveirinha, A. Salandrino, and N. Engheta, "Epsilon-near-zero metamaterials and electromagnetic sources: tailoring the radiation phase pattern," Phys. Rev. B **75**(15), 155410 (2007).
21. M. Silveirinha and N. Engheta, "Tunneling of electromagnetic energy through subwavelength channels and bends using ε-Near-Zero materials," Phys. Rev. Lett. **97**(15), 157403 (2006).

#198113 - $15.00 USD Received 23 Sep 2013; revised 8 Nov 2013; accepted 12 Nov 2013; published 15 Nov 2013

22. J. Luo, P. Xu, H. Chen, B. Hou, L. Gao, and Y. Lai, "Realizing almost perfect bending waveguides with anisotropic epsilon-near-zero metamaterials," Appl. Phys. Lett. **100**(22), 221903 (2012).
23. I. C. Khoo, D. H. Werner, X. Liang, A. Diaz, and B. Weiner, "Nanosphere dispersed liquid crystals for tunable negative-zero-positive index of refraction in the optical and terahertz regimes," Opt. Lett. **31**(17), 2592–2594 (2006).
24. N. M. Litchinitser, A. I. Maimistov, I. R. Gabitov, R. Z. Sagdeev, and V. M. Shalaev, "Metamaterials: electromagnetic enhancement at zero-index transition," Opt. Lett. **33**(20), 2350–2352 (2008).
25. J. B. Pendry and S. A. Ramakrishna, "Focusing light using negative refraction," J. Phys. Condens. Matter **15**(37), 6345–6364 (2003).
26. Y. Lai, H. Chen, Z. Q. Zhang, and C. T. Chan, "Complementary Media Invisibility Cloak that Cloaks Objects at a Distance Outside the Cloaking Shell," Phys. Rev. Lett. **102**(9), 093901 (2009).
27. W. Yan, M. Yan, and M. Qiu, "Generalized compensated bilayer structure from the transformation optics perspective," J. Opt. Soc. Am. B **26**(12), 32–35 (2009).
28. W. Yan, M. Yan, and M. Qiu, "Generalized nihility media from transformation optics," J. Opt. **13**(2), 024005 (2011).
29. J. B. Pendry, L. Martín-Moreno, and F. J. García-Vidal, "Mimicking surface plasmons with structured surfaces," Science **305**(5685), 847–848 (2004).
30. F. J. García-Vidal, L. Martín-Moreno, and J. B. Pendry, "Surface with holes in them: new plasmonic metamaterials," J. Opt. A, Pure Appl. Opt. **7**(2), S97–S101 (2005).
31. S. Xiao, Q. He, X. Huang, and L. Zhou, "Super imaging with a plasmonic metamaterial: role of aperture shape," Metamaterials (Amst.) **5**(2–3), 112–118 (2011).
32. J. Bravo-Abad, F. J. García-Vidal, and L. Martín-Moreno, "Resonant transmission of light through finite chains of subwavelength holes in a metallic film," Phys. Rev. Lett. **93**(22), 227401 (2004).
33. Here one can also impose the condition that the two systems exhibit the same transmission properties, although the mathematics are a bit complicated.
34. CONCERTO 7.0, developed by Vector Fields Ltd, England (2008).
35. To estimate the working bandwidth, we define the frequencies at which the transmittance of our sample decreases to 0.5 as two boundaries of the working range.

1. Introduction

Controlling electromagnetic (EM) waves at will has always been fascinating, but conventional materials exhibit limited abilities to achieve this aim. Transformation optics (TO) theory, proposed independently by J. Pendry *et al.* [1] and U. Leonhardt [2] in 2006, is a powerful tool to engineer the EM space so as to control the flow of light at a desired manner. Since its establishment, many fascinating wave-manipulation phenomena have been predicted based on the TO theory, such as invisibility cloaking [1,2], illusion optics [3,4], field rotator/shifter /transformer [5–7], chirality switching [8], image transformer [9] and hyperlensing [10]. However, to realize these predicted effects, the EM space should be filled with certain inhomogeneous/anisotropic materials, which are hard to realize by naturally existing materials but have to rely on metamaterials (MTM).

MTMs are artificial materials composed by subwavelength microstructures with tailored EM responses, which exhibit exotic optical properties not existing in nature. Although MTMs have enabled realizing certain physical effects including negative refraction [11,12], subwavelength imaging [13,14], and more recently anomalous reflection/refraction [15,16], still, a large body of TO-based devices are hard to realize with MTMs. The inherent difficulty is that those TO devices require the filling materials to exhibit extreme EM parameters (either very large or very small) which are hard to realize with current technologies. As a result, the number of experimental demonstrations is much smaller than available theoretical proposals. It is thus highly desired to realize certain TO media employing the MTM concept, based on which the TO predictions can be verified.

In this work, we describe a practical way to achieve a certain type of TO medium—"optic-null medium" (ONM), which presents an optically non-existing space, and experimentally demonstrate several applications of the ONM. We first briefly describe the physical concept of an ONM and its interesting properties (Sec. 2), and then introduce our approach to practically realize such a medium (Sec. 3). Specifically, we develop an effective medium theory (EMT) based on the rigorous mode-expansion method to successfully retrieve the effective EM parameters of the proposed system, and employ full wave simulations to demonstrate that such a medium can indeed mimic an ONM optically. Finally, we perform

#198113 - $15.00 USD Received 23 Sep 2013; revised 8 Nov 2013; accepted 12 Nov 2013; published 15 Nov 2013

both experiments and simulations to illustrate several applications of the ONM in Sec. 4, and conclude our paper in Sec. 5.

2. Physical concept and basic properties of the optics-null medium

The key idea of the TO theory is to link the medium filling the physical space with a coordinate transformation, which is, in turn, dictated by a certain operation on space [1–10]. In this paper, we consider the operation of stretching a space of near-zero thickness (denoted as Δ in Fig. 1(a)) to a space of finite-thickness (denoted by b in Fig. 1(b)). Based on the TO concept, the path of a light ray will make a conformal change after this operation. Therefore, in the limit of $\Delta \to 0$, when a light ray passes though such a space (with thickness b), it should follow the straight line without any distortion and phase accumulation as if the space does not exist optically. The requested TO medium to realize such an operation is thus called an ONM, which represents an optically non-existing space (see Fig. 1(c)).

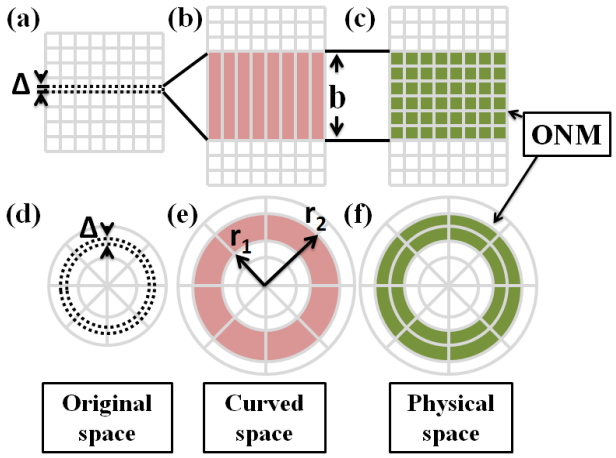

Fig. 1. Coordinate transformation that stretches an original flat space with thickness Δ ((a) and (d)) to a final space with thickness of b ((b) and (e)), which can in turn be replaced by a flat space filled with the optics-null medium ((c) and (f)). The upper row corresponds to Cartesian coordinate and the lower row to cylindrical coordinate.

According to the TO theory [1], it is straightforward to derive the EM parameters of the ONM (shown in Fig. 1(c)) as

$$\ddot{\varepsilon} = \ddot{\mu} = \begin{pmatrix} \Delta/b & 0 & 0 \\ 0 & \Delta/b & 0 \\ 0 & 0 & b/\Delta \end{pmatrix} \xrightarrow{\Delta \to 0} \begin{pmatrix} 0 & 0 & 0 \\ 0 & 0 & 0 \\ 0 & 0 & \infty \end{pmatrix} \tag{1}$$

in which the last expression is valid for the limiting case of $\Delta \to 0$. Here the permittivity and permeability tensors are written based on Cartesian coordinate system, where the matrix index $i = 1,2,3$ represent x, y, z, respectively. The same technique can be applied to the cylindrical coordinate system, where the operation is to stretch a zero-thickness (along the radial direction) space (Fig. 1(d)) to a finite-thickness space (Fig. 1(e)). In this case, the required ONM (Fig. 1(f)) filling the physical space should have the following EM parameters [10],

$$\ddot{\varepsilon} = \ddot{\mu} = \begin{pmatrix} \infty & 0 & 0 \\ 0 & 0 & 0 \\ 0 & 0 & 0 \end{pmatrix}, \tag{2}$$

#198113 - $15.00 USD Received 23 Sep 2013; revised 8 Nov 2013; accepted 12 Nov 2013; published 15 Nov 2013

where the matrix index $i = 1,2,3$ represent r, θ, z, respectively.

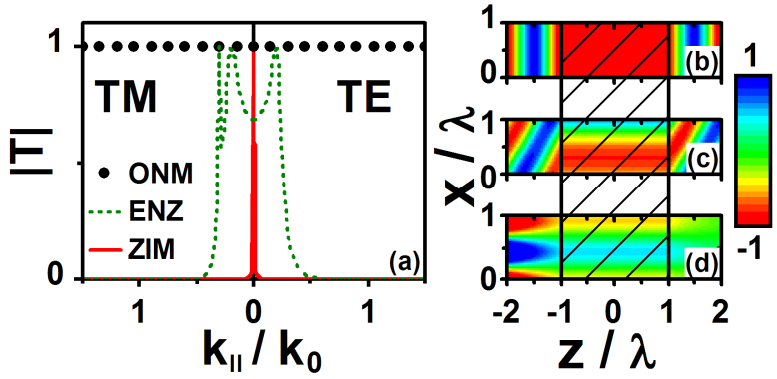

Fig. 2. (a) FEM-computed transmission amplitudes $|T|$ for EM waves with different incident angle and polarization passing through a 2λ-thick slab of ONM (solid circles), ENZ (green dash line, with $\varepsilon = 0.1$) or ZIM (red line), correspondingly. (b)-(d) FEM simulated electric field (E_y) distributions for TE-polarized EM waves passing through a 2λ-thick ONM slab with parallel wave-vectors: (b) $k_x = 0$ (c) $k_x = 0.5k_0$ and (d) $k_x = 1.2k_0$. Here, k_0 is the wave-vector in vacuum and the shadow areas represent the ONM.

To visualize the key properties of an ONM, we performed full-wave simulations based on the finite-element method (FEM) [17] to study the ONM described by Eq. (1). In our simulations, we shined plane waves with different incident angle and polarization onto a slab of ONM and then computed the transmission/reflection coefficients as well as the field distributions. We took very large values for ε^z and μ^z to mimic ∞ in our simulations [18]. We found that in all cases studied, the incident plane waves transmit perfectly through the ONM without any reflections, independent of the incident angle and polarization (see solid circles in Fig. 2(a)). In addition, field distributions (see Figs. 2(b)–2(d)) show that the transmitted waves do not acquire any phase accumulations, as if the ONM does not exist at all [19]. Note that this conclusion is valid even in the case of an evanescent wave excitation (see Fig. 2(d)) where the field amplitude keeps at a constant value inside the ONM. Therefore, when a source is placed on the front surface of an ONM, every Fourier components radiated from the source can perfectly transmit through the ONM, and the re-interference of those transmitted waves will form an image which is an exact replica of the source, on the exit plane of the ONM. Such a super-lensing effect is actually a straightforward consequence of the stretch operation as depicted in Fig. 1, since the "source" and "image" represents the same point in the original space. We emphasize that an ONM is fundamentally different from an epsilon-near-zero (ENZ) material {with $\varepsilon \to 0, \mu = \mu_0$} [20–22] and an isotropic zero-index material (ZIM) {$\varepsilon = \mu = 0$} [23,24]. As shown in Fig. 2(a), both ENZ and ZIM are perfectly transparent only for certain incident angles but induce strong reflections in most other cases, including particularly the cases of evanescent wave excitations. The inherent physics is that the impedance does not match in an ENZ and ZIM material under general incidence conditions.

We note that an ONM can also be realized by combining a slab of ordinary material with a carefully chosen negative-index material slab, based on the idea of complementary medium [25–28]. However, so far it is still a great challenge to practically realize a high-quality negative-index material, and thus it is even more difficult to homogenize such a bilayer system to achieve the desired ONM effect.

#198113 - $15.00 USD Received 23 Sep 2013; revised 8 Nov 2013; accepted 12 Nov 2013; published 15 Nov 2013

3. Practical realization of the ONM

Although an ONM exhibits very attractive optical properties, how to realize it remains a great challenge for MTM researchers due to its extreme EM parameters required (0 and ∞). Instead of combining different EM resonant units to achieve such extreme parameters, here we demonstrate that a specific photonic system can well *mimic* an ONM. The system is schematically depicted in Fig. 3(a), which is a holey metallic plate (HMP) [29–32] with subwavelength apertures arranged in a square lattice with periodicity d. Here we only consider the microwave frequency domain so that metallic can be treated as a perfect electric conductor (PEC). The aperture can take any *symmetrical* complex shape as long as the resonance wavelength associated with it is much longer than its own size (i.e., $\lambda >> d$). We first extend a previously established EMT for simple-shaped aperture case [30] to a general situation. Symmetry argument tells us that the effective permittivity/permeability tensor of the MTM should be

$$\ddot{\varepsilon}_{\text{eff}} = \varepsilon_0 \begin{pmatrix} \varepsilon_{\text{eff}}^{\parallel} & 0 & 0 \\ 0 & \varepsilon_{\text{eff}}^{\parallel} & 0 \\ 0 & 0 & \varepsilon_{\text{eff}}^{\perp} \end{pmatrix}, \ddot{\mu}_{\text{eff}} = \mu_0 \begin{pmatrix} \mu_{\text{eff}}^{\parallel} & 0 & 0 \\ 0 & \mu_{\text{eff}}^{\parallel} & 0 \\ 0 & 0 & \mu_{\text{eff}}^{\perp} \end{pmatrix}. \quad (3)$$

In what follows, we determine the 4 unknowns ($\varepsilon_{\text{eff}}^{\parallel}$ $\varepsilon_{\text{eff}}^{\perp}$ $\mu_{\text{eff}}^{\parallel}$ $\mu_{\text{eff}}^{\perp}$) by requesting that the two systems (e.g., model and the realistic one) exhibit the same optical responses with respect to general excitations (see Fig. 3(b)), under certain approximations.

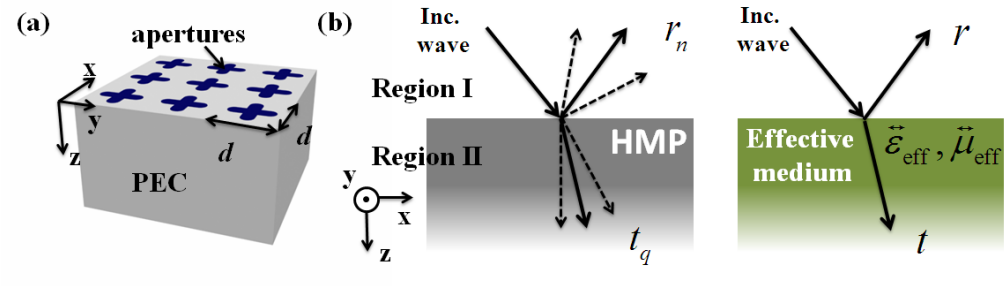

Fig. 3. (a) Geometry of a HMP. (b) Scheme of mapping a HMP to a homogeneous anisotropic effective medium.

Suppose that the realistic system is illuminated by a transverse-electric (TE) - polarized light with a parallel wave vector $k_{\parallel}^{0}\hat{x}$. The scattering properties of such a system can be solved by the standard mode-expansion method [30–32]. Wave in region I can be expressed as $\vec{E}^{I} = \vec{E}_{\text{S}}^{\text{in}} + \sum_n r_n \vec{E}_{S}^{\text{ref},n}$, where $\vec{E}_{\text{S}}^{\text{in}}$ represents the TE-polarized incident plane wave and $\vec{E}_{S}^{\text{ref},n}$ the reflected plane waves along the n-th diffraction channel (with $k_{\parallel}^{n} = k_{\parallel}^{0} + n\pi/d$) with reflection coefficient r_n. **H** field can be derived from the **E**-field easily. Meanwhile, **E**-field in region II can be expressed as $\vec{E}^{II} = \sum_q t_q e^{i\vec{k}_{\parallel}\cdot\vec{R}_j}\vec{E}_{q}^{\text{WG}}$ when $\vec{r}$ is inside an aperture located at $\vec{R}_j$ and is 0 elsewhere, where t_q is the expansion coefficient for the q-th waveguide mode with wave-function given by $\vec{E}_{q}^{\text{WG}}$. For general aperture shapes, while it is difficult to obtain analytical expressions for $\vec{E}_{q}^{\text{WG}}$, one can always employ numerical simulations to get $\vec{E}_{q}^{\text{WG}}$ for each mode. An important property of these eigenmodes is that they are orthogonal to each other. Again, **H**-field in this region can be derived from the **E**-

#198113 - $15.00 USD Received 23 Sep 2013; revised 8 Nov 2013; accepted 12 Nov 2013; published 15 Nov 2013

field easily. By matching the boundary conditions at the interface located at $z = 0$ and fully utilizing the orthonormal properties of these eigenmodes, we can in principle determine all the coefficients r_n, t_q [30,31]. However, the final expressions of these coefficients are quite complicated and physically less transparent.

We now take two approximations to derive an analytical solution for the given problem, based on which the effective parameters can be obtained. First, we retain only the fundamental modes in both regions (i.e., the specular reflection in region I and the fundamental waveguide mode inside the aperture) but neglect all the high-order modes. This single-mode approximation is widely used and is physically sound here since we assume $\lambda >> d$ so that all high-order modes are evanescent waves. Under this approximation, we found that the specular reflection coefficient is written as

$$r_0 = \frac{\left|S_0\right|^2 k_z^{\text{air}} / k_z^{\text{WG}} - 1}{\left|S_0\right|^2 k_z^{\text{air}} / k_z^{\text{WG}} + 1}, \tag{4}$$

in which

$$\left|S_0\right|^2 = \frac{\left|\int_{u.c.} d\vec{r}_{\parallel} \left(\vec{E}_{\parallel}^{\text{in}}\right)^* \cdot \vec{E}_{0,\parallel}^{\text{WG}}\right|^2}{\int_{u.c.} d\vec{r}_{\parallel} \left|\vec{E}_{\parallel}^{\text{in}}\right|^2 \cdot \int_{u.c.} d\vec{r}_{\parallel} \left|\vec{E}_{0,\parallel}^{\text{WG}}\right|^2} \tag{5}$$

represents the overlapping between the incident plane wave $\vec{E}_{\parallel}^{\text{in}}$ and the fundamental waveguide mode $\vec{E}_{0,\parallel}^{\text{WG}}$. Here only the parallel field components are relevant, and the integrals are performed within a unit cell. $k_z^{\text{air}}, k_z^{\text{WG}}$ are the z-components of **k** vectors of waves in different regions. Explicitly,

$$k_z^{\text{WG}} = \sqrt{\varepsilon_h}\sqrt{\omega^2 - \omega_c^2} / c, \tag{6}$$

where ε_h is the relative permittivity of the medium filling the aperture and ω_c is the cut-off frequency of the fundamental waveguide mode, again obtainable by numerical simulations for general aperture cases.

In principle, S_0 depends on the incident angle. However, such angular dependence is very weak here since the variation of incident field across the aperture area is weak when the aperture is deep-subwavelength in size. Therefore, we adopt the second approximation to neglect such angular dependence and assume that S_0 can be calculated under normal-incidence condition. For rectangle-shaped aperture, we get from Eq. (5) that $S_0 = 2\sqrt{2}a / \pi d$, recovering previous result obtained analytically [30]. In general complex-shaped apertures, S_0 can be easily calculated by numerical simulations after $\vec{E}_{0,\parallel}^{\text{WG}}$ has been solved.

We now derive the effective-medium parameters of the structure. Under exactly the same external illumination, we find that the reflection coefficient of the *model* system (i.e., the anisotropic MTM) is

$$r = \frac{\mu_{\text{eff}}^{\parallel} k_z^{\text{air}} / k_z^{\text{MTM}} - 1}{\mu_{\text{eff}}^{\parallel} k_z^{\text{air}} / k_z^{\text{MTM}} + 1}, \tag{7}$$

where

$$k_z^{\text{MTM}} = \sqrt{(\omega / c)^2 \varepsilon_{\text{eff}}^{\parallel} \mu_{\text{eff}}^{\parallel} - k_{\parallel}^2 \mu_{\text{eff}}^{\parallel} / \mu_{\text{eff}}^{\perp}} \tag{8}$$

#198113 - $15.00 USD Received 23 Sep 2013; revised 8 Nov 2013; accepted 12 Nov 2013; published 15 Nov 2013

is the z-component of the **k** vector for a TE-polarized wave traveling inside such an anisotropic MTM. The effective-medium parameters can be fixed by equating Eqs. (7) and (8) with Eqs. (4) and (6) [33]. A careful analysis tells us that

$$\begin{aligned} \varepsilon_{\text{eff}}^{\parallel} &= \left(1-\omega_c^2/\omega^2\right)\varepsilon_h/\left|S_0\right|^2 \\ \mu_{\text{eff}}^{\parallel} &= \left|S_0\right|^2 \\ \mu_{\text{eff}}^{\perp} &= \infty \end{aligned} \quad . \tag{9}$$

Similar calculations for transverse-magnetic (TM) - polarized excitations can give us the values of $\varepsilon_{\text{eff}}^{\parallel}, \mu_{\text{eff}}^{\parallel}, \varepsilon_{\text{eff}}^{\perp}$. For $\varepsilon_{\text{eff}}^{\parallel}, \mu_{\text{eff}}^{\parallel}$, the TM calculations yield the same expressions as recorded in Eq. (9), which justified our TE calculations independently. Meanwhile, we get additionally from the TM calculations that

$$\varepsilon_{\text{eff}}^{\perp} = \infty. \tag{10}$$

Note that $\varepsilon_{\text{eff}}^{\perp} = \mu_{\text{eff}}^{\perp} = \infty$ is physically understandable, since a bulk medium of our system does not allow EM waves to propagate along a direction within the xy-plane, due to the existence of PEC walls separating different apertures.

Set the working frequency as the waveguide cut-off ($\omega = \omega_c$), we find that

$$\ddot{\varepsilon}_{\text{eff}} = \varepsilon_0 \begin{pmatrix} 0 & 0 & 0 \\ 0 & 0 & 0 \\ 0 & 0 & \infty \end{pmatrix}, \ \ddot{\mu}_{\text{eff}} = \mu_0 \begin{pmatrix} \left|S_0\right|^2 & 0 & 0 \\ 0 & \left|S_0\right|^2 & 0 \\ 0 & 0 & \infty \end{pmatrix}. \tag{11}$$

Therefore, if we can design a HMP exhibiting $\left|S_0\right|^2 \to 0$, then such a system (at the frequency $\omega = \omega_c$) can well mimic an ONM optically, since it exhibits almost identical optical responses as an ONM under excitations with arbitrary polarizations and incident angles.

It is helpful to discuss what kind of aperture shape can better achieve the desired functionality. Apparently, such an aperture should exhibit $\left|S_0\right|^2 \to 0$ and deep-subwavelength response ($\lambda_c >> d$ with λ_c being the cut-off wavelength), simultaneously. Unfortunately, the simple square shape is not a good choice. According to the analytical expression $S_0 = 2\sqrt{2}a/\pi d$ for a square-shape aperture, we need $a/d \to 0$ to make $\left|S_0\right|^2 \to 0$. However, in such a case ε_h would be extremely large to satisfy the second condition $\lambda_c >> d$ (Note $\lambda_c = \sqrt{\varepsilon_h}a$). Alternatively, we find that the fractal-like aperture shape is a much better choice (see Fig. 4(a)), because the line width *w* of such structure is an *additional* and *independent* parameter to control the overlapping integral $\left|S_0\right|^2$, without affecting the deep-subwavelength property of the whole aperture shape [31].

#198113 - $15.00 USD Received 23 Sep 2013; revised 8 Nov 2013; accepted 12 Nov 2013; published 15 Nov 2013

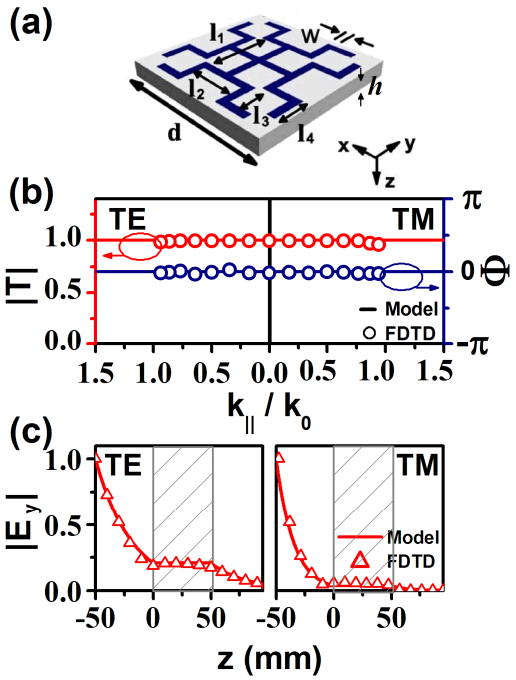

Fig. 4. (a) Designed HMP slab with parameters d = 20 mm, l_1 = 10 mm, l_2 = 5 mm, $l_3 = l_4$ = 4 mm, w = 1 mm and h = 50 mm. (b) Transmission amplitudes (red line and circles, left axis) and phases (blue line and circles, right axis) for EM waves with different parallel wave-vector and polarization passing through the designed HMP (circles, calculated by FDTD simulations) and the corresponding effective-medium slab (lines). (c) Distributions of $|E_y|$ along z-axis for the system shined with a TE-polarized incident evanescent wave with $k_{||} = \pi/3d$ (left panel) and a TM-polarized incident evanescent wave with $k_{||} = \pi/2d$ (right panel), calculated by FDTD simulations ($|E_y|$ is averaged over a unit cell) for realistic HMP (triangles) and the effective-medium slab (lines). Here, the shadow areas represent the HMP, and the working frequency is 2.0 GHz in all calculations.

Assuming $\varepsilon_h = 4$, we performed finite-difference-time-domain (FDTD) simulations [34] to study the EM properties of the fundamental-mode (i.e., cut-off frequency and field distribution) for such an aperture, and found that $\omega_c = 2\pi \times 2.0$ GHz and $|S_0|^2 = 0.047$. We put the calculated $|S_0|^2$ into Eq. (11) and then obtain the effective-medium model for this HMP (with thickness h = 50 mm). Lines in Fig. 4(b) represent the transmission amplitude $|T|$ and phase Φ for plane EM waves passing through such a slab with different incidence angle and polarization, calculated based on the effective-medium model at $\omega = \omega_c$. We next employed FDTD simulations to study the transmission behaviors of the *realistic* system at $\omega = \omega_c$, and found that the obtained $|T|$ and Φ spectra under propagating-wave incidence (open circles in Fig. 4(b)) are in excellent agreement with the model results. We found that the same behaviors hold for evanescent-wave excitations although it is difficult to directly calculate the $|T|$ and Φ. As an illustration, we show in Fig. 4(c) the FDTD-simulated electric field distributions (averaged over a unit cell area) for evanescent-wave excitations with different polarizations. The obtained data (open triangles) are in perfect agreement with the effective-medium model results (lines), justifying our effective-medium model. More importantly, while the E-fields outside the HMP slab decay exponentially, the field amplitude keeps constant inside the HMP slab in both cases, which is the key feature of the ONM.

#198113 - $15.00 USD Received 23 Sep 2013; revised 8 Nov 2013; accepted 12 Nov 2013; published 15 Nov 2013

4. Experimental verifications and applications of ONM

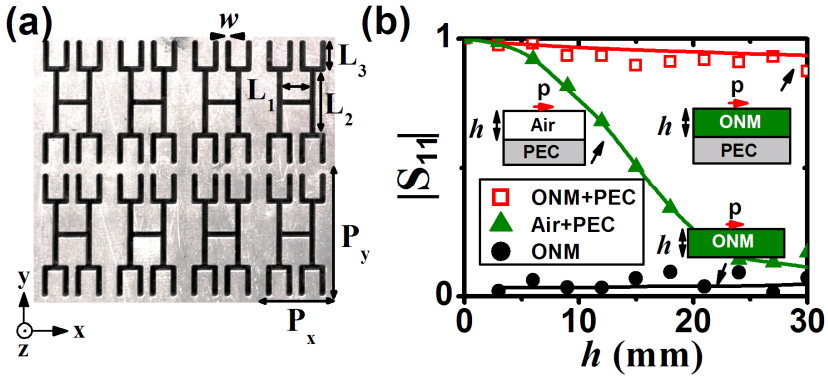

Fig. 5. (a) Picture of the fabricated sample with parameters L_1 = 12 mm, L_2 = 13 mm, L_3 = 6 mm, P_x = 18 mm, P_y = 31 mm, w = 1 mm (b) Return loss ($|S_{11}|$) spectra of a dipole antenna put on top of standing-alone ONM slabs (black), ONM slabs backed by a PEC substrate (red) and air gaps backed by a PEC substrate (green), obtained by experiment (symbols) and FDTD simulations (lines). Here the working frequency is 2.63 GHz.

In this section, we fabricate realistic ONM structures based on the theory described in last section, and experimentally demonstrate a couple of applications of such systems. Instead of using the *isotropic* fractal-like aperture as in Fig. 4, here we chose an *anisotropic* fractal-like shape (see Fig. 5(a)) to design and fabricate our ONM. Our EMT can be easily extended to such anisotropic cases, where ω_c, $|S_0|^2$ can take different values for $\{\varepsilon_{\text{eff}}^{\text{x}}, \mu_{\text{eff}}^{\text{y}}\}$ and $\{\varepsilon_{\text{eff}}^{\text{y}}, \mu_{\text{eff}}^{\text{x}}\}$ dictated by different waveguide modes polarized along x or y directions. In certain applications with fixed in-plane **E** directions (see below), such anisotropic aperture shape is enough since the incident waves can only detect a certain set of parameters. We can thus utilize this property to design a *deep-subwavelength* aperture within a confined area, even without using high-index insertions.

For the designed aperture, we performed FDTD simulations to study its fundamental-mode (for $\vec{E} \parallel \hat{y}$) properties and found that $\omega_c = 2\pi \times 2.63$ GHz and $|S_0|^2 = 0.07$. Therefore, at the working frequency $\omega = \omega_c$, the effective parameters of this system are $\varepsilon_{\text{eff}}^{\text{y}} = 0$, $\varepsilon_{\text{eff}}^{\text{z}} = \infty$, $\mu_{\text{eff}}^{\text{x}} = 0.07\mu_0$, $\mu_{\text{eff}}^{\text{z}} = \infty$, according to the EMT described in last section. We then fabricated a series of HMP slabs with different thicknesses and performed microwave experiments to demonstrate several fascinating properties/applications of such systems.

The first experimental demonstration is the "radiation cancellation effect". As shown in the inset to Fig. 5(b), suppose we place a dipole antenna (length = 16.5 mm) on top of an ONM slab with thickness h, which is in turn put on a perfect-electric-conductor (PEC) substrate. Since an ONM represents "optically" nothing, it appears that the dipole antenna is placed *directly* on top of the PEC. Thus, the dipole antenna cannot radiate at all due to image cancellation effect, so that its return loss should approach to 1 (i.e., $|S_{11}|$ = 1). In our experiments, we used a vector network analyzer (Agilent E8362C) to test the radiation properties of the antenna at the frequency 2.63 GHz. Varying the thickness h of the HMP slab, we found that the measured $|S_{11}|$ (open squares) of the antenna remains essentially at ~1. FDTD simulations performed on the realistic systems (red line) are in good agreements with the experimental results, which unambiguously demonstrated the "radiation cancellation" effect as predicted. We next performed a series of control experiments by replacing the HMP slabs by air gaps with the same thicknesses. The measured $|S_{11}|$ (green triangles) varies continuously from 1 to 0 as h increases from 3 to 30 mm, which is in perfect agreement with FDTD simulations (green line). Such an effect is expected since the cancellation of the dipole with its image is affected by the propagating phase inside the air gap, and thus the

#198113 - $15.00 USD Received 23 Sep 2013; revised 8 Nov 2013; accepted 12 Nov 2013; published 15 Nov 2013

cancellation is good only when $h \to 0$. As a final test, as we removed the PEC substrate, we found that the return loss of the antenna is nearly zero as if the slabs do not exist, again in good agreement with FDTD simulations as well as the expectations based on the ONM.

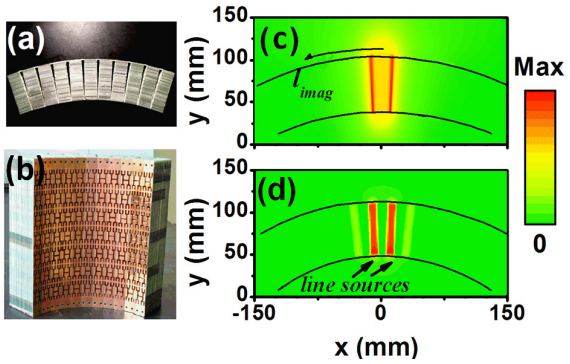

Fig. 6. (a) Top-view and (b) side-view pictures of the experiment sample. $|\mathbf{E}/\mathbf{E}_{ref}|$ distributions for the hyperlensing effect realized by (c) a cylindrical ONM with parameter given by Eq. (2) and (d) our designed sample obtained by FDTD simulations at frequency 2.63 GHz.

Finally, we experimentally demonstrated a particular application of the ONM, which can work as a hyperlens as predicted in [10]. The working principle is shown in Fig. 6(c). Put two line sources on the inner surface of a cylindrical-shaped ONM layer, FDTD simulations show that the image formed on the outer surface of the ONM is just the original source magnified by a factor of $R_{\text{out}}/R_{\text{in}}$, with $R_{\text{out}}, R_{\text{in}}$ denoting the radii of the outer and inner surfaces, respectively. Such a hyperlensing effect is a straightforward consequence of the "stretching" operation as depicted in Fig. 1. To fabricate the cylindrical ONM, we cut a 65mm-thick HMP slab (with the same parameters as in Fig. 5(a)) into 18 mm-wide stripes (each containing 7 unit elements) and then arrange them into a cylindrical shape. Adjacent stripes are metallically connected to avoid wave tunneling effects. Figures 6(a) and 6(b) show the top-view and side-view pictures of the sample. The inner and outer radii of the realized sample are 235 and 300 mm, respectively, and samples with other radii can be easily fabricated. It is straightforward to derive the effective-medium parameters of such a cylindrical HMP. We find that, at the working frequency, $\ddot{\varepsilon}$ of our system is identical to that of a cylindrical ONM (Eq. (2)) and $\ddot{\mu}$ is very close to that of a cylindrical ONM with only μ_θ slightly modified by a metric term but still approaching to zero. We have performed FDTD simulations on the designed realistic sample to study the hyperlensing effect at the frequency 2.63 GHz. Figure 6(d) depicts the calculated field distribution on the central xy-plane of the realistic sample, which is in excellent agreement with the field distribution of the ideal cylindrical ONM (Fig. 6(c)).

#198113 - $15.00 USD Received 23 Sep 2013; revised 8 Nov 2013; accepted 12 Nov 2013; published 15 Nov 2013

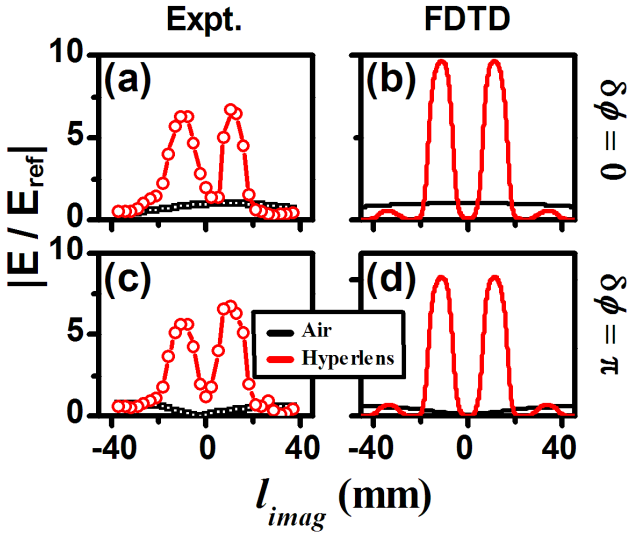

Fig. 7. (a,c) Measured and (b,d) simulated $\left|\mathbf{E}/\mathbf{E}_{ref}\right|$ distributions at the outer surface of the hyperlens when two dipole antennas are placed on the inner surface of the hyperlens, fed by in-phase ((a) and (b)) and out-of-phase ((c) and (d)) signals. Black lines/symbols correspond to the case of replacing the sample by air. In both measurements and simulations, the $|\mathbf{E}|$ value at the position l_{imag} = 0 mm in the in-phase case is taken as the reference $\left|\mathbf{E}_{ref}\right|$.

In our experiments, we used two identical monopole antennas (length = 8 mm) as the source and another identical one as the probe. The two source antennas are fed with equal-amplitude signals with a particular phase difference $\delta\phi$ controlled by a phase shifter. Still set the working frequency as 2.63 GHz, we placed two monopoles on the inner surface of the device, separated by a distance 18 mm ($\sim\lambda/6$), and then measured the field distribution on the image plane (exit surface of the hyperlens). As important references, we first measured the field distributions formed on the image plane when the hyperlens was removed, in two particular cases where two antennas are in phase and out of phase. The obtained results are depicted as black squares in Figs. 7(a) and 7(c), respectively. We note that the two sources cannot be distinguished on the image planes in both cases, consistent with theoretical expectation since they are within a subwavelength region ($<\lambda/2$). Meanwhile, the field distributions are highly dependent of $\delta\phi$, and the $\left|\mathbf{E}/\mathbf{E}_{ref}\right|$ is maximized (minimized) when $\delta\phi$ equals to 0 (π). We next studied the cases when the hyperlens was added. From the measured distributions shown as solid circles in Figs. 7(a) and 7(c), we found that now the two monopoles can be clearly distinguished on the image plane, with measured half-maximum width of each peak being roughly 20 mm $\sim\lambda/6$. More importantly, now the separation of two peaks is 23 mm, which is enhanced by a factor of ~ 1.3 as compared to the original value 18 mm, and the field at the image peak is enhanced significantly (more than 7 times) than that without the hyperlens.

All these features are consistent with the theoretical predictions based on an ONM. FDTD simulations were performed on the realistic system, and the obtained results (lines in Figs. 7(b) and 7(d)) are in good agreement with the experimental ones. However, the working band width of our fabricated ONM is quite narrow, which is only 0.05GHz for the 65 mm-thick sample estimated by FDTD simulations [35]. As the working frequency significantly deviates from the waveguide cut-off, the effective permittivity of our sample will change dramatically from zero so that our device cannot work as an ONM.

#198113 - $15.00 USD Received 23 Sep 2013; revised 8 Nov 2013; accepted 12 Nov 2013; published 15 Nov 2013

Two things are worthy being mentioned. First, our experiments demonstrated that the hyperlensing effect is independent of $\delta\phi$ (see Figs. 7(a) and 7(c)), which is the desired result according to the "stretching" operation (see Fig. 1). Such an interesting property offers the ONM more freedoms in future applications. Second, although the magnification factor is only ~1.3 in present demonstration, this factor can be easily improved by increasing the curvature or the thickness of our device. FDTD simulations were performed on a thicker sample (with realistic structure) with $R_{\text{out}} / R_{\text{in}} \approx 2$ to demonstrate this point. Put two sources separated by 0.32λ at the inner surface of this new ONM, FDTD simulations show that the resulting images formed on the outer surface are separated by a distance $\sim 0.64\lambda$, which can now be distinguished in the far field (see Fig. 8).

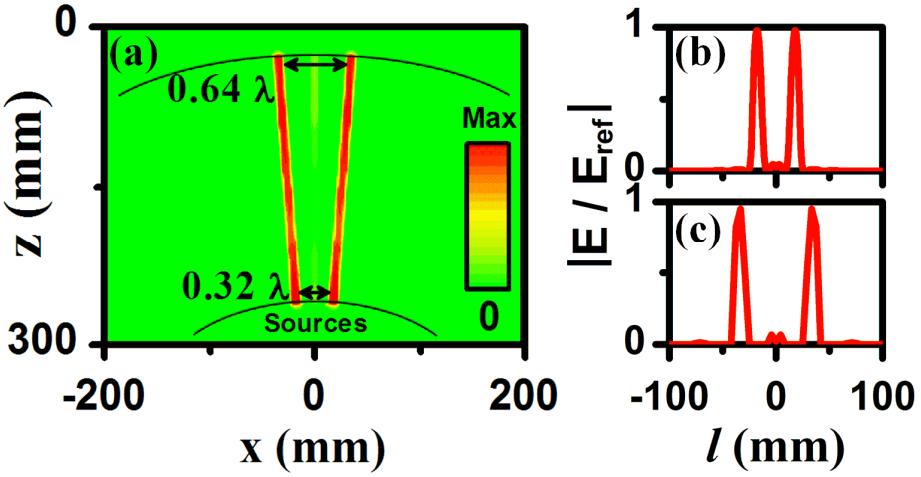

Fig. 8. FDTD simulated $\left|\mathbf{E} / \mathbf{E}_{ref}\right|$ distributions on the (a) x-z plane, (b) source plane, and (c) image plane for the hyperlensing effect realized by a cylindrical ONM with $R_{out} = 475\,\text{mm}$ and $R_{in} = 235\,\text{mm}$ at the working frequency 2.63 GHz.

5. Conclusions

In summary, based on an extended effective medium theory, we designed and fabricated a realistic structure to mimic the optical-null medium, and experimentally demonstrated several interesting physical effects and applications of such a system. Experimental results are in excellent agreement with full-wave simulations and model analyses. More applications can be expected for such a system.

Acknowledgments

This work was supported by NSFC (60990321, 11174055, 11204040), the Program of Shanghai Subject Chief Scientist (12XD1400700) and MOE of China (B06011). Q. He acknowledges financial supports from China Postdoctoral Science Foundation (2012M520039, 2013T60412).

#198113 - $15.00 USD Received 23 Sep 2013; revised 8 Nov 2013; accepted 12 Nov 2013; published 15 Nov 2013